International Conference on Space Optics—ICSO 2022

Dubrovnik, Croatia

3–7 October 2022

Edited by Kyriaki Minoglou, Nikos Karafolas, and Bruno Cugny,

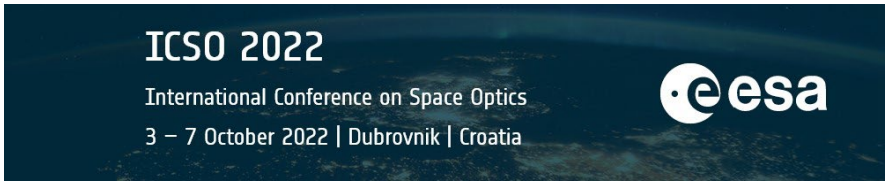

Albedo bias reduction for Nanocarb GHG sensor : comparison of panchromatic or hyperspectral ancillary imager, and high finesse or multiple harmonics Fabry-Perot interferometer

International Conference on Space Optics — ICSO 2022, edited by Kyriaki Minoglou, Nikos Karafolas, Bruno Cugny, Proc. of SPIE Vol. 12777, 1277771 · © 2023 ESA and CNES · 0277-786X · doi: 10.1117/12.2691374

Albedo bias reduction for Nanocarb GHG sensor : comparison of panchromatic or hyperspectral ancillary imager, and high finesse or multiple harmonics Fabry-Perot interferometer

Yann Ferrec*[a], Laurence Croizé[a], Pierre-Yves Foucher[b]
[a]Onera, centre de Palaiseau, France ;
[b]Onera, centre de Toulouse, France

ABSTRACT

Nanocarb is an imaging spectrometer dedicated to the monitoring of greenhouse gases, especially carbon dioxide (CO_2). Nanocarb system is based on an array of static Fabry-Perot interferometers, the free-spectral range of which being adapted to the periodicity of the spectral signature of the gas target. A challenge of Nanocarb is to provide an accurate and precise estimation of the total column of gas, and a limiting factor may be uncertainty on the albedo (or surface reflectance) estimation. We investigate several tracks to limit this effect, especially by reducing correlation between albedo and gas concentration estimation. Four solutions have been identified. The first two are to estimate albedo independently from Nanocarb, with an additional imaging system (panchromatic or hyperspectral). The last two are to modify the design of the Fabry-Perot interferometers to acquire with Nanocarb albedo information less influenced by gas concentration. In particular, a higher finesse leads to an improved precision on CO_2 scale factor estimation.

Keywords: greenhouse gases, GHG, hyperspectral

1. NANOCARB GHG SENSOR

Global and frequent (intraday) monitoring of greenhouse gases (GHG) is increasingly required to better model climate changes, especially to discriminate sources and sinks of GHG, and to help public policies of GHG reduction. Space measurement can provide such a global and frequent coverage, a constellation of about 25 satellites ensuring a revisit of half-a-day. However, due to budget constraints, such a mission should rely on small satellites and hence very compact payloads. These payloads consists in an instrument directly sensitive to GHG concentration, completed with an instrument dedicated to aerosol measurement, since it is recognized that aerosol estimation is a key element to improve the quality of GHG concentration retrieval from space optical measures [1]. During the H2020 Scarbo project [2][3], two such compact payloads were studied, the one for aerosol being SpexOne, from SRON [4] and the one focusing on GHG being Nanocarb.

Nanocarb is a very compact imaging spectrometer, developed by Grenoble-Alpes University (UGA) and Onera in France [5]. Nanocarb has three key features (summed up on Figure 1 from [6]).

- Nanocarb is based of an array of static Fabry-Perot interferometers, each interferometer having its specific thickness and being associated with a microlens, to perform snapshot spectral imaging (multicam configuration [7]).
- The Fabry-Perot interferometers are used in a multiplex mode, that is, their free spectral range is far narrower than the spectral sensitivity domain. In other words, each pixel integrates several peaks of the Fabry-Perot transmission function: Nanocarb thus does not directly measure the spectrum, but an interferogram, which makes Nanocarb close to Fourier-transform spectrometers [8][9].
- The third key feature of Nanocarb is to measure not the whole interferogram, but rather to focus only on a few optical path differences (OPD), adapted to the periodicity of the spectral signature of the gas. Indeed, GHG gas like CO_2, CH_4, N_2O, SO_2, and so on, have spectral signatures with roughly equally spaced lines. Consequently, in the Fourier space, information is concentrated on small regions, which are targeted by Nanocarb. This allows to acquire high spectral resolution information with very few OPDs, typically a few tens of OPDs.

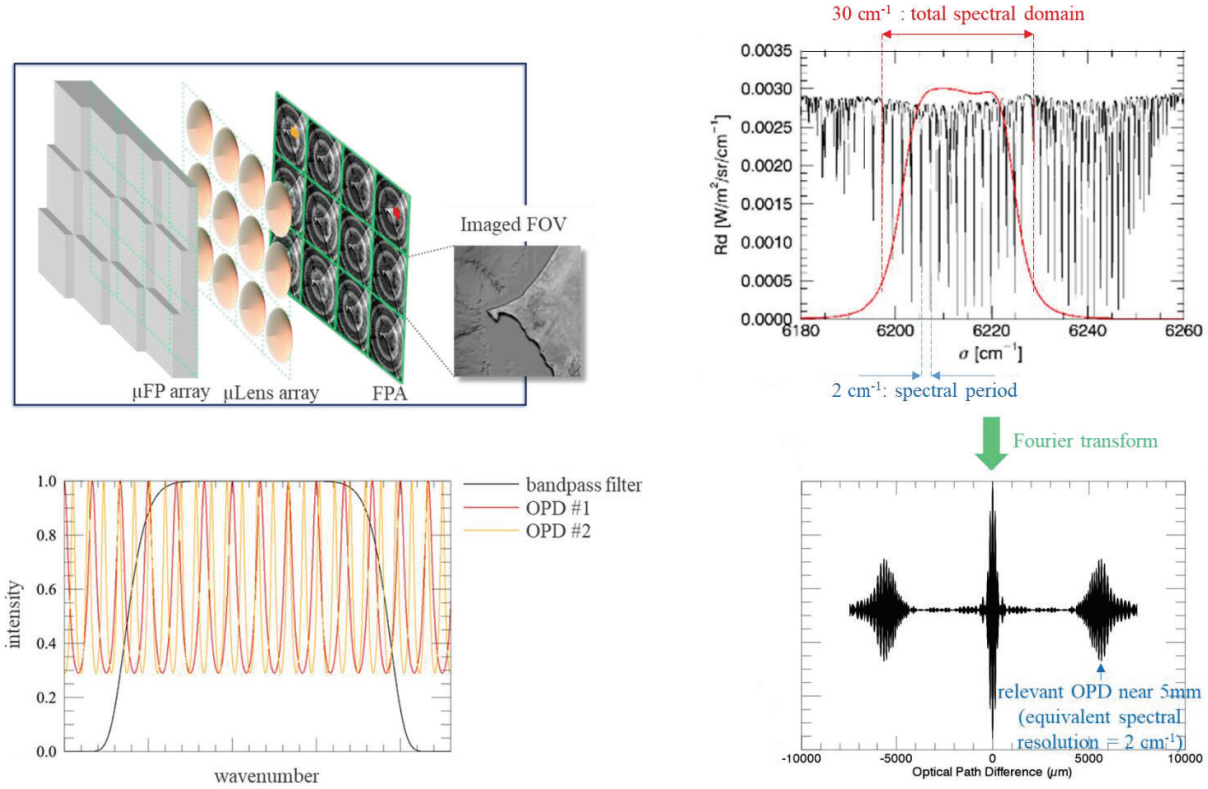

Figure 1. Summary of Nanocarb principle. Top left: main optical components of Nanocarb, with an array of micro Fabry-Perot interferometers, a lenslet array, and a common focal plane array (FPA), on which are a set of images of the scene, each modulated by the Fabry-Perot rings. However, the significant point is that each Fabry-Perot has its own thickness: interference rings are unnecessary (and may even be undesirable). Bottom left: spectral transmittance of Nanocarb, for two pixels marked on the top-left figure. These two pixels are associated with two distinct Fabry-Perot interferometers, and thus two distinct optical path differences (therefore the periodicity of the spectral transmission functions are different). With low-finesse Fabry-Perot interferometers, these spectrak ransmittances are roughly sinusoidal, so that Nanocarb is close to a Fourier-transform spectrometer. Top-right: in black, apparent spectral radiance at top-of-atmosphere of a ground point in the spectral region where CO_2 absorbs. CO_2 absorption is responsible for the spectral lines, quite periodic. In red, the bandpass filter to isolate this region. Bottom-right: Fourier transform of the previous spectrum. Most of information is around 5 mm OPD. To detect CO_2 in this spectral region, the Fabry-Perot of Nanocarb have consequently an OPD close to 5 mm.

2. PERFORMANCE ESTIMATION OF A SPACE MISSION BASED ON A FIRST NANOCARB DESIGN

During the Scarbo project, a first design of Nanocarb for a space mission was proposed, with an associated performance model on the radiometrically calibrated interferograms (L1 products). These outputs, with their counterparts from Spex, were merged by LMD (*Laboratoire de Météorologie Dynamique*, Palaiseau, France) to assess the quality of the estimated total GHG column (CO_2 and CH_4), called L2 product. These results were then used by Noveltis (France), SRON and the University of Bremen (Germany) to model the quality of the fluxes are local and regional scales (L4 products), but this is out the scope of this proceeding. We briefly recall in the next subsections this first Nanocarb design for a space mission, and the main results of the L2 performance estimation. More details can be found in [10][11][12].

2.1 First Nanocarb design

The Nanocarb payload consists in 4 cameras, each one dedicated to a specific spectral band where the targeted gas presents quasi-periodic lines: B1 for O_2, B2 for CO_2, B3 for CH_4, and B4 also for CO_2. The choice of these four spectral bands based on published design of other instruments, like CarbonSat ([13] table 5.3) or CO2M ([14]), but with a spectral range

reduced to fit with the periodicity of the lines. From these spectral bands, relevant OPDs were selected, with a simple radiometric model [10], and with the requirements to maximize signal dependency to CO_2 while minimizing dependency to H_2O, and taking into account spectral shift of the narrow band filter and of the Fabry-Perot interferometer with incidence angle. The resulting spectral bands and OPD intervals are given in Table 1.

Table 1. The four spectral bands of Nanocarb (first design): spectral ranges and OPDs

band name	B1	B2	B3	B4
target	O_2, surface pressure, aerosol	CO_2, H_2O	CH_4	CO_2
central wavenumber	13093 cm^{-1} (764 nm)	6213 cm^{-1} (1610 nm)	6078 cm^{-1} (1645 nm)	4840 cm^{-1} (2066 nm)
Full Width at Half Maximum	35 cm^{-1} (2.0 nm)	24 cm^{-1} (6.2 nm)	69 cm^{-1} (18.7 nm)	18 cm^{-1} (7.7 nm)
central OPDs	0.6 mm, 1.8 mm	2.3 mm, 5.6 mm	1.0 mm, 2.0 mm	5.8 mm, 11.7 mm

2.2 Main results from the L2 performance estimation

L2 performance estimation was performed in a simplified way [11], as it was evaluated on 324 scenarios corresponding to different values for 5 observation parameters: scene albedo (ALB), solar zenithal angle (SZA), height (CLH) and optical depth (COD) of a coarse aerosol layer, and optical depth of a fine aerosol layer (FOD). Interferograms from the 4 spectral bands were simulated thanks to an instrumental model of Nanocarb, and retrieval was performed jointly on the four spectral bands. In other words, what we call interferogram is actually the concatenation of the four interferograms provided by each Nanocarb camera. Retrieval was done according to the optimal estimation approach [15], with only 10 variables in the state vector: 3 scaling factors of H_2O, CO_2 and CH_4 vertical profiles, surface pressure, 4 albedos (one for each spectral band), and 2 aerosol optical depths (for the coarse and fine modes). SpexOne data were used through an a-priori estimation of the aerosol parameters and the associated uncertainties. An important point is that the errors were calculated not for a single Nanocarb frame, but taking into account the numerous frames where a ground point appear: indeed, as Nanocarb is a 2D snapshot imager, a ground point is seen by successive frames, while it goes across the field-of-view. This significantly increases the amount of data available and thus reduces random error.

The main results of this L2 performance estimation is summed-up on Figure 2, reproduced from [12][1]: it shows that with the current Nanocarb design, precision better than 1 ppm for XCO2 and 6 ppb for CH4 are attainable. Obviously, this conclusion has to be slightly qualified. On one hand, the performance evaluation was done with simplifying hypothesis, for instance on the vertical profiles (including temperature), on the spectral variation of albedos, on measure noises, and so on. On the other hand, the Nanocarb design will be improved from the results of this L2 performance evaluation, especially by refining the selection of the spectral bands and of the OPDs. However, this L2 product study also emphasized another point to be improved, which is the correlation between gas concentration and albedo estimations. This is the topic we will discuss in the next of this proceeding.

[1] For sake of clarity, we discarded from this figure the sensitivity to uncertainties of SpexOne product (see p. 4850 from [12] for more details on this aspect).

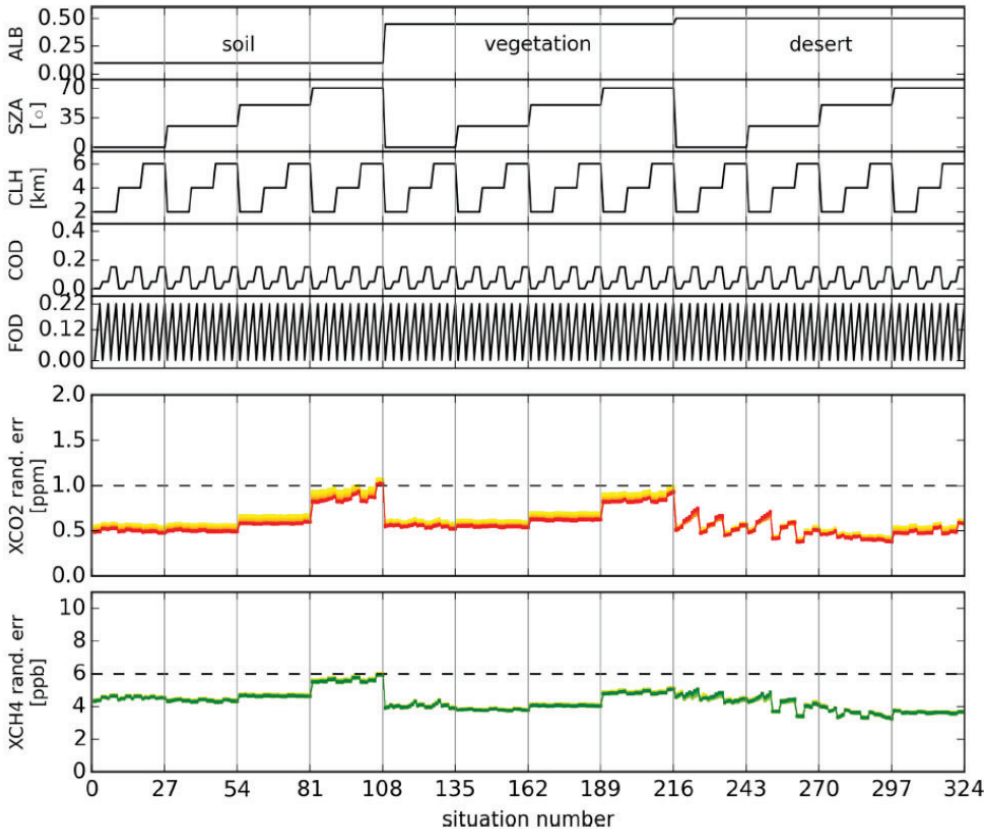

Figure 2. Nanocarb random errors on the column-averaged dry-air mole fractions of CO_2 (XCO2) and CH_4 (XCH4), for the 324 scenarios. The top five plots give the values of the observation parameters defining the scenarios, and the two bottom plots give the random error on XCO2 and XCH4, taking into account SpexOne results in the retrieval process. This figure is extracted from [12]: see this reference to have more details and analysis.

3. CORRELATION BETWEEN ALBEDO AND GAS CONCENTRATION ON THE INTERFEROGRAM

3.1 Preliminary remark

The illustrations below are made with simulated spectra calculated with 4AOP radiative transfer code [16]. Main simulation parameters are listed in Table 2. Some of these parameters differ from the ones used in [11] or [12], that is why a direct comparison with the numerical results that can be found in these references has to be done caustiously: especially, the nominal CO_2 concentration is different, we do not consider aerosol, integration time is reduced, and in this proceeding we focus only on band B2. Our goal is indeed to describe tracks to reduce the correlation between albedo and XCO2 estimation, not to provide a thorough analysis of the system performance.

3.2 Methodology

The very common approach to retrieve the geophysical parameters from the measured interferograms is to minimize a merit function with two terms: a data fidelity term, and a regularization term, to take into account a-priori knowledge on these parameters. Here, we will neglect this latter term, since we focus on the instrumental model. Thus, under common simplifying assumptions on the noise (normal distribution), the merit function is the square of the Malahanobis distance between the measured interferogram and the simulated one. Furthermore, we assume that noise is decorrelated with the same standard deviation s for each OPD, so that the merit function χ^2 to minimize is merely:

$$\chi^2(p) = \sum_{i=1}^{N} \left(\mathcal{I}(p, \delta_i) - I_{mes}(\delta_i)\right)^2$$

with p the parameter vector, $\mathcal{I}(p, \delta_i)$ the simulated interferogram at OPD δ_i, and $I_{mes}(\delta_i)$ the measured (and noisy) interferogram. If we note K the Jacobian matrix, that is

$$K[i,j] = \left.\frac{\partial \mathcal{I}}{\partial p_j}\right|_{(p,\delta_i)}$$

then it can be shown that the covariance matrix $\hat{S}$ on the retrieved parameters is given by:

$$\hat{S} = s^2 \cdot [K^t \cdot K]^{-1}$$

with K being calculated at the a-posteriori value for p, but we assume that is identical to K calculated at the true position.

The square-root of diagonal elements of $\hat{S}$ give the standard-deviation on the estimation of the parameters, and the non-diagonal elements give the correlation between these parameters.

Table 2. Main parameters used for the simulation

parameter	**value**
scene	
atmosphere	AFRL2 except for CO_2
XCO_2 (nominal scenario)	415 ppm
aerosol	none
albedo (nominal scenario)	0.2
Solar Zenithal Angle (SZA)	50°
view	nadir
optics	
f-number	4.8
transmission (except from Fabry-Perot)	0.95
waveband	B2 (around 6213 cm^{-1})
Fabry-Perot material	Silicon
number of OPDs N_{OPD}	64
OPD ranges	[2.1 ; 2.95] mm (25 OPDs) [5.5 ; 5.9] (39 OPDs)
FPA	
pixel size	15 µm
read-out noise	170 e-
dark current	none
quantum efficiency	0.9
system	
integration time	40 ms
number of frames M	80

Another (but equivalent) way to obtain this result is to compare $\chi'(p, p_{true})$ the distance between $\mathcal{I}(p, \delta)$ and $\mathcal{I}(p_{true}, \delta_i)$ – p_{true} being the true set parameters – with $\mathcal{s}$, the "blur" radius due to noise around $\mathcal{I}(p_{true}, \delta_i)$. When $\mathcal{I}(p, \delta)$ is closer to $\mathcal{I}(p_{true}, \delta_i)$ than $\mathcal{s}$, p would become a likely parameter. In the vicinity of p_{true}, $\chi'^2(p, p_{true})$ is the quadratic form of matrix $K^t \cdot K$: the orientation of its eigenvectors indicate the correlation between the parameters. With only two parameters in the state vector, it is thus very easy to visualize the correlation between these two parameters. This is our case, since to focus on correlation between albedo and CO_2 scale factor, we restrict our state vector to albedo and a scale factor on the CO_2 vertical profile.

3.3 Correlation between albedo and CO_2 scale factor for the first Nanocarb design in band B2

Let us take the example of the first Nanocarb design, with the filter and the OPDs defined in [11] (but limited to band B2). On Figure 3 we plotted $\chi'^2(p, p_{true})$ normalized by $\left(s/\sqrt{M}\right)^2$, the variance of the noise level improved by the M multiple observations.

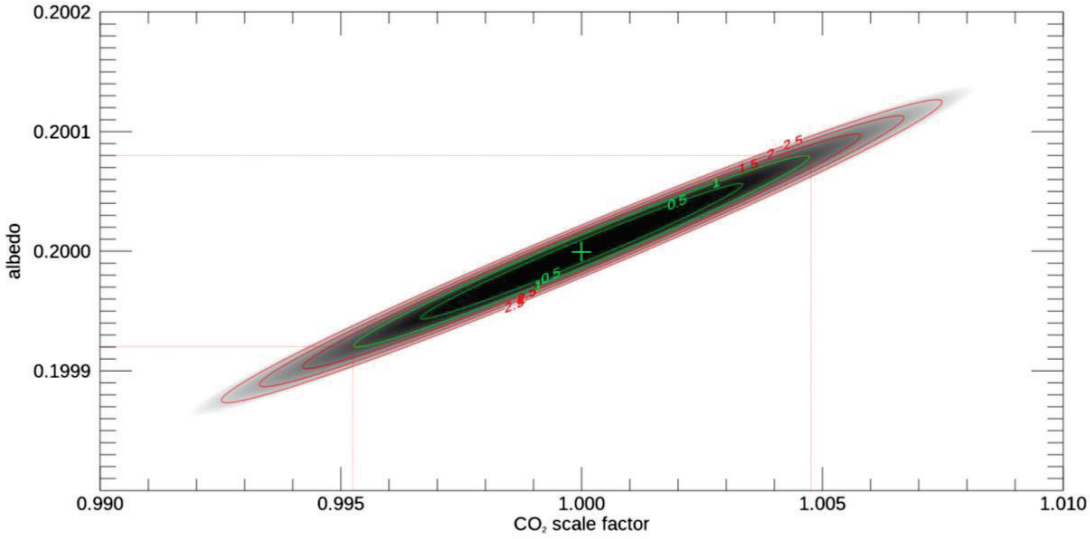

Figure 3. $\chi'^2(p, p_{true})$ normalized by $\left(s/\sqrt{M}\right)^2$. p_{true} is a scale factor of 1 and an albedo of 0.2 (green cross). Bandpass filter and OPD distribution are those of the first Nanocarb design, the integration time is 40 ms (see Table 1 and Table 2).

We clearly see the correlation between albedo and CO_2 concentration: the axes of the quadratic form are slanted with respect to the parameters (albedo , CO_2 scale factor) axes: if we choose state vectors on the major axis of the ellipse, they may produce very similar interferograms, roughly indiscernible compared to the noise, up to a CO_2 scale factor of 1.0048, or 2 ppm[2] (see Figure 4, bottom, green plot). This is far larger than the width of the χ'^2 function taken at constant albedo: if the albedo were known, the random error on CO_2 scale factor would be greatly reduced (see Figure 4, bottom, red plot: if the albedo were known, this interferogram would not be likely copared with the noise level).

[2] this is larger than the 0.5 ppm of Figure 2, but we remind that the scenarios are not the same (see Section 3.1)

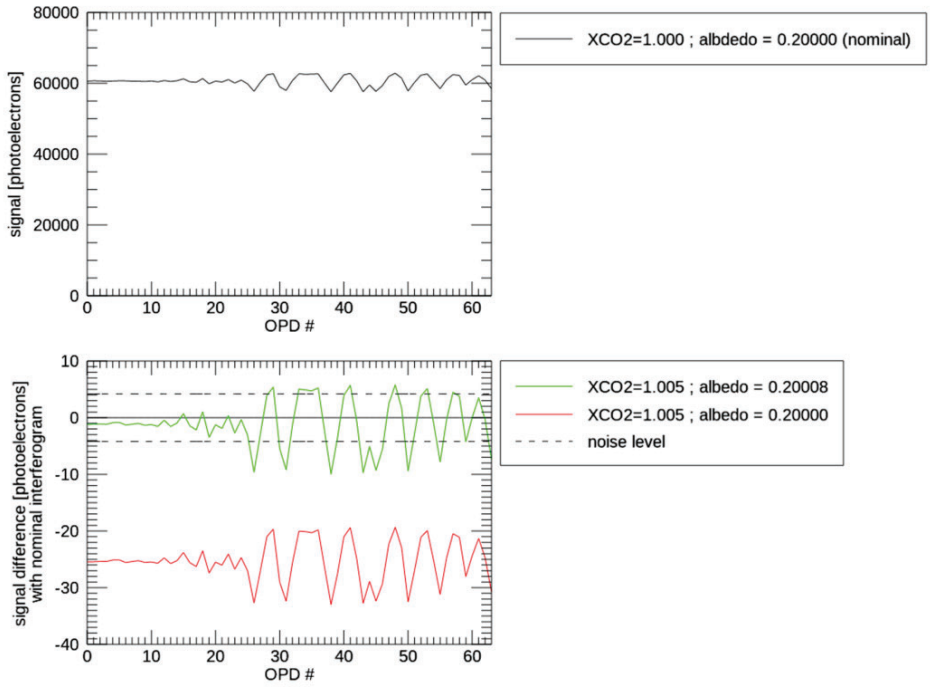

Figure 4. Top: simulated interferogram in the nominal scenario. Bottom: difference with this nominal interferogram for two sets of the state vector. The noise level is $\mathcal{s}/\sqrt{M \cdot N_{OPD}}$ to take into account the joint inversion of the N_{OPD} OPDs of the interferogram and the noise reduction due to accumulation of M frames. Note that performing retrieval only on the modulated part of the interferogram (that is the fringe amplitude) makes the results far worse: we could then no more separate CO_2 scale factor and albedo, what we can do when conserving the DC part, since their impact on the DC part and on the modulated part are not identical.

It is thus desirable to reduce this correlation between albedo and CO_2 concentration, either to reach better precision on CO_2 estimation, or, at constant precision, to simplify the payload. In the next section, we propose possible solutions to this problem.

4. PROPOSITIONS TO REDUCE CORRELATION BETWEEN ALBEDO AND GAS CONCENTRATION

To deal with this difficulty of the correlation between albedo and gas concentration, we could consider solutions based on pure processing of Nanocarb images. It could be for instance a joint retrieval of the whole pixels of the image[3], with regularization conditions on albedo and CO_2 spatial texture, like Total Variation (TV) regularization on the albedo image (to deal with edges), and smoother regularization function on CO_2. However, we will not consider such solutions, to focus on hardware improvement.

We listed two approaches: the first one is to add an imager dedicated to albedo estimation. This is a similar solution to the one brought to the problem of aerosol, with the presence of SpexOne, the output of which (aerosol information) being an input for Nanocarb retrieval. The second approach is to modify the Nanocarb interferometer, to reduce correlation at the very interferogram level.

[3] or a posteriori correction, taking into account the correlated correction between albedo and CO_2

4.1 Panchromatic or hyperspectral ancillary imager

The goal here is to estimate albedo with more information than the one provided by Nanocarb, which means that a panchromatic imager in exactly the same spectral band than Nanocarb would be of no use[4]. On the contrary, an hyperspectral imager would bring information at other wavelengths. It would thus allow to estimate the spectral slope of albedo to interpolate it in Nanocarb spectral bands. Furthermore, a visible and shortwave infrared (SWIR) hyperspectral camera would also improve Spex aerosol estimation at 1.6 µm. The main difficulty is the precision (and probably accuracy) required on the estimated albedo: for instance, with the scenario described at Section 3.3, precision on albedo has to be better than 0.1%. Another difficulty is that adding an hyperspectral camera compliant with this requirement would probably make the payload considerably heavier, and we would therefore lose one of the main asset of Nanocarb, its compacity.

A panchromatic camera would be more adapted as a compact payload, but the limit is that a very narrow spectral band, to be out of the CO_2 signature, will lead to a very low signal-to-noise ratio (SNR), while a broader spectral band would not bring more information than Nanocarb. Thus, a multispectral camera may be a good trade-off, to estimate the spectral slope of surface reflectance around the Nanocarb spectral band, while maintaining a high SNR and a low dependency to CO_2 or other trace gas content.

4.2 Multiple harmonics and higher finesse interferometer

Rather than relying on an additional camera, we can also try to reduce intrinsic sensitivity of Nanocarb to albedo. In this first analysis, we choose not to change neither the spectral band nor the number of OPDs (i.e. the number of micro-lenses of the Nanocarb camera), to focus only on the interferometer level. There are thus two free parameters: the plate thickness (i.e. the OPDs), and the surface reflectivity (i.e. the interferometer finesse).

About the choice of OPDs, we could dedicate some of them to higher harmonics of the gas signature: they are still sensitive on CO_2 and to albedo, but the ratio of dependency to these parameters may be different from the OPDs at the fundamental frequency, which could lead to a better separation of the parameters. Nevertheless, fringe contrast decreases as the harmonics increases, and the whole performance of the system is worse. For instance, if the twenty last OPDs are around 11.2 mm rather than 5.6 mm, the standard deviation on the CO_2 scale factor increases to 0.006, instead of 0.005 for the initial set of OPDs.

Changing the surface reflectivity seems more promising. Indeed, if we increase the surface reflectivity (i.e. the finesse of the interferometer), the baseline of the spectral transmission of the Fabry-Perot interferometer tends to zero. Consequently, the signal at the OPDs where the peaks of the Fabry-Perot spectral transmission do not coincide with the CO_2 spectral lines does not depend (or only slightly) on CO_2 concentration, but only on albedo. On the contrary, at OPDs where the peaks of the Fabry-Perot spectral transmission do coincide with the CO_2 spectral lines, the signal contain as much information as with low finesse interferometer[5]. The limit is that the total measured signal decreases as the finesse increases. There is thus an optimal finesse, as it appears on Figure 5. In the studied configuration, with a finesse about 5, the standard deviation on the CO_2 scale factor decreases to 0.004, but this exact optimal finesse may depend on the scenario (scene and system).

[4] for our current topic (for instance, a high resolution imager may be helpful for raw image processing, but it is out of the scope of this proceeding)
[5] as long as the width of the Fabry-Perot spectral transmission are broad with respect to the CO_2 spectral lines.

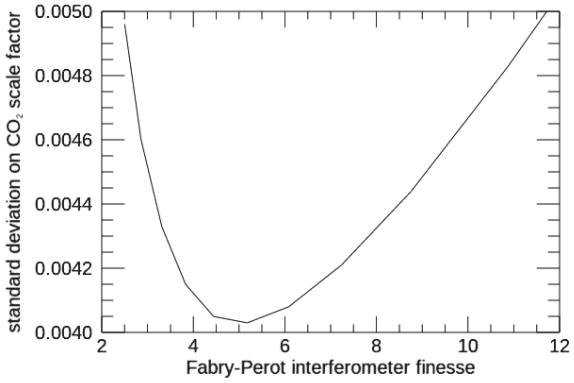

Figure 5. Error on CO_2 scale factor vs finesse of the Fabry-Perot interferometer, for the same scenario than defined on Table 2.

5. CONCLUSION

Current performance of Nanocarb is limited by the correlation between albedo and CO_2 concentration. To overcome this limitation, a solution would be to use an ancillary camera, either hyperspectral (if we also want to increase aerosol correction) or multispectral (if we focus only on albedo estimation). The drawback of such a solution is to make a payload more cumbersome. Thus, another way would be to change the parameters of the Fabry-Perot interferometer at the heart of Nanocarb, and especially by increasing its finesse. In this current study, restricted to the spectral band around 1.6 µm, we showed that with a finesse equal to 5 rather than 2.5, the error on CO_2 scale factor is decreased by 20%. A more thorough study will be conducted, both to confirm these results on more scenarios and to optimize Nanocarb spectral band and OPD definition.

REFERENCES

[1] Ruslie, S. P., Hasekamp, O., aan de Brugh, J., Fu, G., Meijer, Y. and Landgraf, J., "Anthropogenic CO_2 monitoring satellite mission: the need for multi-angle polarimetric observations," *Atmos. Meas. Tech.*, 14, 1167–1190 (2021).
[2] https://scarbo-h2020.eu/
[3] Brooker Lizon-Tati, L., Val Serra, S., Bovensmann, H., Crevoisier, C., Dogniaux, M., Croizé, L., Ferrec, Y., Le Coarer, E., Gousset, S., Sic, B., Smit, M. and the Scarbo consortium, "SCARBO: A constellation of small satellites for the monitoring of anthropogenic greenhouse gases," *Proc. 73rd International Astronautical Congress IAC* IAC-22-B1.2.1 (2022).
[4] van Amerongen, A., Rietjens, J., Campo, J., Dogan, E., Dingjan, J., Nalla, R., Caron, J. and Hasekamp, O., "SPEXone: A compact multi-angle spectro-polarimeter," *Proc. ICSO 2018*, SPIE 11180, 111800L (2018).
[5] Ferrec, Y., Bonnery, G., Brooker, L., Croizé, L., Gousset, S., Le Coarer, E. and the Scarbo consortium, "NanoCarb part 1: Compact snapshot imaging interferometer for CO2 monitoring from space," *Proc. ICSO 2018*, SPIE 11180, 1118021 (2018).
[6] Ferrec, Y., de la Barrière, F., Croizé, L., Gousset, G., Le Coarer, E. and Rodrigo, J., "Overview of the Nanocarb GHG sensor project," *Proc. Optro 2022*, 99 (2022)
[7] Tanida, J., Kumagai, T., Yamada, K., Miyatake, S., Ishida, K., Morimoto, T., Kondou, N., Miyazaki, D. and Ichioka, Y., "Thin observation module by bound optics (TOMBO): concept and experimental verification," *Appl. Opt.* 40, 1806-1813 (2001).
[8] Rommeluère, S., Guérineau, N., Haidar, R., Deschamps, J., de Borniol, E., Million, A., Chamonal, J.-P. and Destefanis, G., "Infrared focal plane array with a built-in stationary Fourier-transform spectrometer: basic concepts," *Opt. Lett.* 33, 1062-1064 (2008).
[9] Pisani, M. and Zucco, M., "Compact imaging spectrometer combining Fourier transform spectroscopy with a Fabry-Perot interferometer," *Opt. Exp.* 17, 8319-8331 (2009).

[10] Gousset, S., Croizé, L., Le Coarer, E., Ferrec, Y., Rodrigo, J. and Brooker, L. for the Scarbo consortium, "NanoCarb hyperspectral sensor: on performance optimization and analysis for greenhouse gas monitoring from a constellation of small satellites," *CEAS Space Journal* 11, 507-524 (2019)
[11] Dogniaux, M., *Suivi de la concentration atmosphérique de CO2 par satellite : performances et sensibilités des prochains concepts d'observation dans le proche infrarouge*, Thèse de doctorat de l'Institut Polytechnique de Paris (2021)
[12] Dogniaux, M., Crevoisier, C., Gousset, S., Le Coarer, E., Ferrec, Y., Croizé, L., Wu, L., Hasekamp, O., Sic, B. and Brooker, L., "The Space Carbon Observatory (SCARBO) concept: assessment of XCO_2 and XCH_4 retrieval performance," *Atmos. Meas. Tech.*, 15, 4835-4858 (2022).
[13] European Space Agency, *Report for Mission Selection: CarbonSat*, ESA SP-1330/1(2015)
[14] Sierk, B., Fernandez, V., Bézy, J.-L., Meijer, Y., Durand, Y., Bazalgette Courrèges-Lacoste, G., Pachot, C., Löscher, A., Nett, H., Minoglou, K., Boucher, L., Windpassinger, R., Pasquet, A., Serre, D. and te Hennepe, F., " The Copernicus CO2M mission for monitoring anthropogenic carbon dioxide emissions from space," *Proc. ICSO 2020*, SPIE 11852, 118523M (2021).
[15] Rodgers, C., *Inverse methods for atmospheric sounding – Theory and Practice*, World Scientific (2000)
[16] https://4aop.aeris-data.fr